Development of wide-angle antenna pattern measurements using a probe-corrected polyplanar near-field measurement technique

S.F. Gregson, C.G. Parini and J. McCormick

Abstract: The authors demonstrate through numerical simulation and experimental measurement that a polyplanar scan geometry consisting of a flat-topped pyramid provides a possible solution to the measurement of high-gain antenna patterns in the forward hemisphere using a planar scanner of size of order 1.5 times the size of the radiating aperture. The importance of correctly determining the normal field component for each partial scan data set is demonstrated and a new auxiliary rotation near-field to far-field transform algorithm is proposed. Additionally it is shown experimentally that by enclosing a medium-gain antenna (e.g. a corrugated horn) within a scan geometry formed by an imaginary box and measuring the near field on all six sides of the box using a suitable rotation of the AUT, a prediction of the full spherical radiation pattern of the antenna can be obtained.

1 Introduction

It is well known that far-field antenna parameters such as pattern, gain, directivity, beamwidth, etc., can be derived using an analytical transformation from measurements taken in the near field [1]. This can be accomplished by representing the field at an arbitrary point in space as an integral over the surface on which the fields are known [2]. Alternatively, considerable computational advantages can be obtained by representing the field as a summation of any elementary wave solutions to Maxwell's equations [3]. Here the coefficients to these solutions are determined by matching the fields on the surface on which the fields are known and by using mode orthogonality. Solving this modal expansion for the fields at an infinite distance from the radiator results in the far-field pattern. A degree of mathematical convenience can be obtained from selecting a modal basis that matches the measurement geometry, i.e. by utilising plane waves for the case where the measurements are taken over a planar surface.

The principal factors in determining the complexity of the near-field to far-field transformation are: the probe directivity pattern correction, the extent of the truncation of the data, the geometry of the surface over which the near field is sampled, and its associated orthogonal modal basis. For the case of the planar near-field methodology, if the forward hemisphere is to be determined exactly, even in the case of a finite aperture, the propagating field must be sampled over a plane of infinite extent. The only exception to this is the nonrealisable case of a finite aperture set in a perfectly conducting ground plane that extends to infinity. Here the sampling interval can collapse to the region of the aperture provided that the samples are taken over a surface that is coincident with the ground plane. In practice, due to the finite extent of the scan plane any conventional planar near-field measurement will inevitably represent a truncated data set, and as such, any predicted far-field pattern would include errors associated with this truncation. Furthermore, the precise nature of this effect is complicated as a variation in any part of the near-field pattern will necessarily, as a consequence of the holistic nature of the transform, result in a change to every part of the corresponding far-field pattern. Importantly, it is the data that is transformed to produce the far-field pattern that is required to be free from excessive truncation. If this data is the product of the combination of a number of partial data sets that, in contrast to the single scan data set, fulfil the transformation requirements in terms of sampling rate and continuity over the sampling interval, then the prediction will be free from truncation errors.

2 Auxiliary translation: conventional strategy

Hitherto the problem of truncation in near-field data acquired over a planar surface has been partially addressed by combining data sets that have been acquired via a series of coplanar transforms, e.g. translations or rotations. The primary truncation error determines the polar angle off boresight out to which any far-field pattern can be predicted from near-field measurements, while the secondary error limits the extent to which the pattern within this angle can be accurately predicted. The primary truncation error can be expressed as the far-field angle of validity [4]

$$Az = \arctan\left(\frac{L_x - a_x}{2d}\right) \quad (1)$$

where L_x denotes the dimension of the scan plane, a_x the dimension of the antenna under test (AUT) and d is the

IEE Proceedings online no. 20045157

doi:10.1049/ip-map:20045157

Paper first received 13th November 2004 and in final revised form 15th August 2005

S.F. Gregson is with BAE Systems, Sensor Systems Division, Crewe Road North, Crewe Toll, Edinburgh EH5 2XS, UK and also with Queen Mary, University of London, Department of Electronic Engineering, Mile End Road, London E1 4NS, UK

C.G. Parini is with Queen Mary, University of London

J. McCormick is with BAE Systems, Sensor Systems Division

E-mail: c.g.parini@elec.qmul.ac.uk

separation between the scan plane and the antenna aperture plane. Partial scans that can be combined to produce the composite data set and will require that the position of the AUT, relative to the scan plane, be spatially transformed between scans so that the combined data set represents a larger scan area than that actually available via a single scan. Clearly, as the actual scan plane of the scanner is at a fixed location it is the AUT that must undergo the spatial transformation. Three common translations are: the AUT is translated in the horizontal, i.e. x, direction between partial scans; the AUT is translated in the horizontal and vertical, i.e. x and y, directions between partial scans; and the AUT is rotated about the normal to the scan plane, i.e. z-axis, between partial scans. If the AUT can be manipulated and repositioned with sufficient accuracy the construction of the combined scans should not involve any loss of accuracy. However, the positional accuracy of the sampling points required to make successful measurements is demanding, i.e. better than a fiftieth of a wavelength in each of the triad of orthogonal directions. This means that the movement of the AUT relative to the scan plane and subsequently its repositioning with the required degree of accuracy for a second or subsequent scan is not a trivial task and requires specialist, potentially costly, precision positioners.

Unfortunately, effective as these techniques undoubtedly are, they necessarily involve spatial translations of the antenna that are dependent on the additional availability of a specialist precision antenna-positioning subsystem. Such subsystems, with the ability to translate the antenna accurately and with sufficient repeatability in a plane tangential to that of the scanner, as a result of the antenna translation occupy significantly large volumes. Additionally the translation of the antenna involves the movement of parts of the RF interference network of the measurement systems, and this will introduce phase errors in the measurements which must be either corrected or minimised. These techniques essentially involve the extension of the size of the existing scan plane by the systematic synthesis of a composite data set from a combination of partial data sets acquired via a series of coplanar translations and/or rotations. However, this strategy, although it can significantly improve the performance of the measurement facility with a minimal increase in computational complexity, can never entirely succeed since any finite number of translations or rotations can never synthesise a plane that is infinite in extent.

3 Auxiliary rotation: basis of an alternative strategy

Techniques for rigorously applying vector isometric rotations to antenna patterns thereby correcting the measurements of misaligned antennas readily offers the possibility of producing antenna measurements based on partial scan techniques that are not coplanar. By rotating the AUT about one or more spatial axes that are not necessarily at a normal to the scan plane and combining the partial scans it is clearly possible to increase the angle of validity and level of accuracy of a planar measurement. The Fig. 1*a* shows the normal alignment and Fig. 1*b* the misalignment of an AUT relative to the scan plane. For the case of the planar near-field to far-field transformation the application of alignment correction data is handled rigorously by expanding the plane-wave spectrum on an irregular grid in the range co-ordinate system (i.e. that system defined by the scan plane). This irregular grid corresponds to a regular grid in the AUT

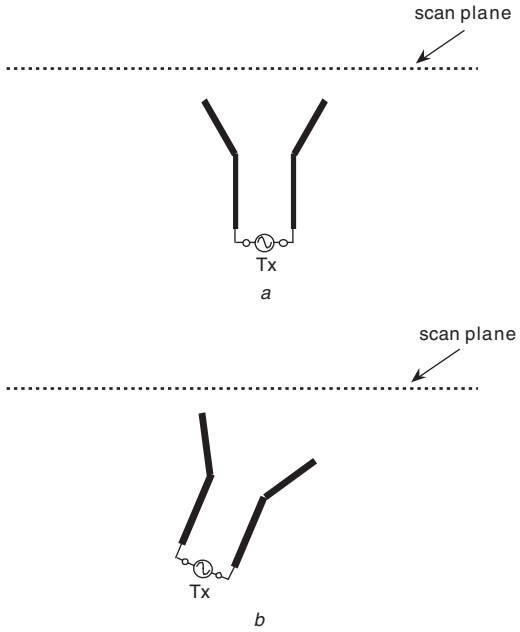

Fig. 1 *Representation of aligned and misaligned antennas*

mechanical co-ordinate system (often taken to be a frame of reference defined by the antenna aperture plane). With the transformation of the measured cartesian field components from the range polarisation basis into the AUT polarisation basis the required isometric rotation is complete.

The probe pattern can be thought of as spatially filtering the fields received from different parts of the AUT. In a planar range, the effects include something similar to a direct multiplication of the far-field probe pattern with the far-field AUT pattern. This can be seen to be a direct result of the nature of the convolution theorem [5] and can be visualised directly from the mechanical operation of the scanner. It is not usually possible to neglect these effects in the planar range because of the large angles of validity required and the short measurement distance employed, c.f. expression for the angle of validity. Considerable care is needed over which co-ordinate system and which field components the probe convolution is understood to have taken place in so that a rigorous deconvolution can be applied. Thus an arbitrary but known probe orientation can be accommodated within our transformation process.

The reconstruction of near-field data over a plane in space other than the measurement plane is accomplished by the application of a differential phase change. This can be seen to be analogous to a defocusing of the far-field image. Near-field data can then be readily reconstructed via the application of a two-dimensional discrete inverse Fourier transform. On this occasion there is no requirement for any additional isometric transformations and as such all of the usual numerical techniques for improving the efficiency of the transformation can be utilised. This reconstructed plane can be located at any of an infinite number of planes that are in the region of space at, or in front of, the AUT's phase centre. It is when the fields are reconstructed at a plane that is coincident with the AUT's 'aperture plane' that this process is of most utility. The antenna aperture can be conveniently thought of as that surface in space which represents the transition between the majority conduction current and displacement current regions defined by the presence of a charge distribution.

Alignment errors manifest themselves in different ways in each domain. If the issues associated with polarisation are

ignored then an error in the AUT to range alignment will correspond to an angular displacement of the far-field pattern. The same error will correspond to a change in the nature of the near-field pattern that is not in general characterised simply by a corresponding linear-phase taper. The acquisition of alignment data is usually based upon the premise of being able to measure the cartesian co-ordinates of four points on the AUT mechanical interface plane in the range co-ordinate system. From these four points we can construct four normals, the average angles between each can be used to indicate the degree of uncertainty in the measurement of these points. The projection of each cartesian component of the first system onto each cartesian component of the second system determines the AUT-to-range direction cosine matrix. For the case where there is a suitable datum available on the antenna the roll angle can be deduced from any of the edge vectors.

In principle these techniques are rigorous, but in practice the integrity of the reconstructed near-field data is not maintained. The source of this error which is propagated through the entire procedure is related to the truncation caused by the differences in the truncation of the measured data sets due to the misalignment of the AUT. Although the process is sufficiently robust to deal with a degree of variation in the truncation of the measured data sets, knowledge of the success of the correction at each stage of the process is crucial. Previously [6] these techniques have been verified by acquiring a low-gain standard-gain horn (SGH) at a variety of different orientations with respect to the range axes. However, the magnitude of the angles through which the patterns were rotated within the transformation process was much smaller that those required by a typical auxiliary rotation system. Hence further verification was required. Thus a planar array antenna, shown in Fig. 2, operating at 9.0 GHz was acquired when aligned to the axes of the range and when rotated in azimuth through ± 15 and $\pm 30^{\circ}$. These angles were chosen as they are thought to be representative of the angles required by typical auxiliary rotation systems. The antenna-to-range alignment information was measured as described, in each case and then used to correct each of the near-field measurements.

These data sets were transformed to the far-field where the radiation patterns were resolved onto a Ludwig III

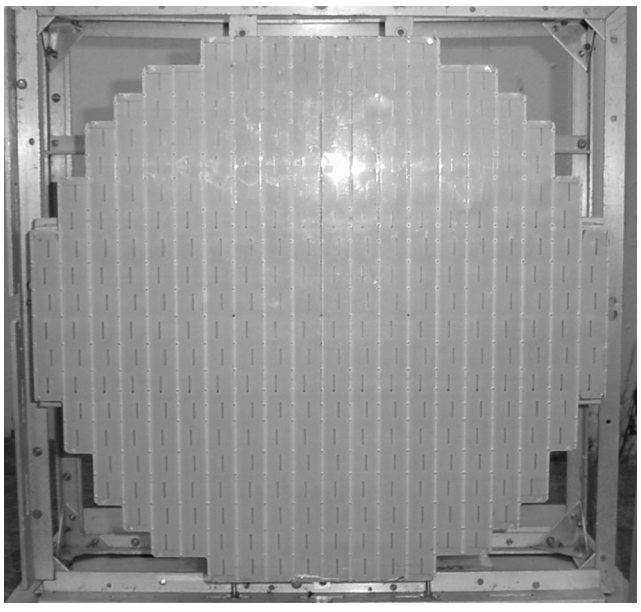

Fig. 2 *Photograph of face of circular array antenna*

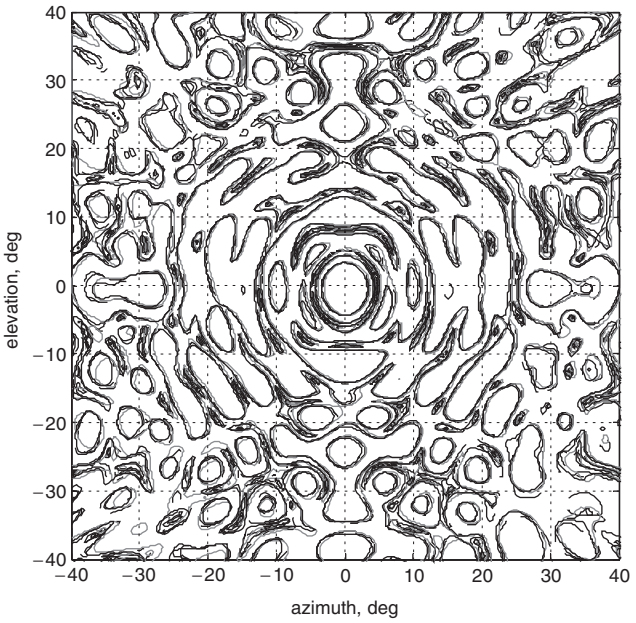

Fig. 3 *Comparison of corrected far-field copolar patterns*

vertical copolarisation and cross-polarisation basis and were tabulated on a regular 151-by-151-element grid in an azimuth over elevation coordinate system. Figure 3 illustrates the degree of agreement attained by presenting the data in the form of overlaid isolevel, i.e. contour, plots so that the differences are illustrated as clearly as possible. Here the contours have been plotted that correspond to the -60, -50, -40, -30, -20 and -10 dB below peak level. A different line-style is used for each data set, where the solid black line is 0°, dotted line is 15°, dashed-dotted line is -15°, dotted line is 30° and grey solid line is -30° cases. These patterns have been plotted out to $\pm 40^{\circ}$ in azimuth and elevation so that the entire far-field data set should be free from first-order truncation effects. Clearly, phenomena associated with the second-order truncation effect remain present within this angular region.

It can be seen that the results are encouraging, as the differences between these far-field radiation patterns are small and subtle in nature. The apparent similarity between the plots suggests that the antenna to range alignment data has been reliably determined and correctly applied. The rigorous application of alignment correction is not limited to that of the plane rectilinear co-ordinate system as these techniques are readily extended to the plane polar and plane bipolar acquisition geometries.

4 Polyplanar technique

Clearly, then, this introduces the possibility of constructing bespoke polyhedral measurement surfaces that enclose the antenna under test and that are designed to be more amenable for the derivation of wide-angle antenna performance from measurements made using existing, possibly smaller, planar near-field measurement facilities. This technique facilitates a reduction in the number of near-field acquisition points relative to a conventional planar measurement with an equal angle of validity, while retaining the mathematical and computational simplicity that is usually associated with the plane-wave spectrum method and planar probe pattern correction.

4.1 Biscan auxiliary rotation technique

In general it is difficult to obtain closed-form solutions for the electromagnetic field at a point in space from knowledge of the tangential electric or tangential magnetic fields over a closed surface for anything but the simplest cases. This is especially true when the closed surface is not coincident and synonymous with the aperture of the radiating structure, as is the case for near-field antenna measurements. As such, recourse to alternative, typically numerical, methods for verification is unavoidable. To this end the near-field measurement geometry was simulated using a uniformly illuminated, purely y-polarised rectangular aperture cut from an infinitely thin perfectly conducting sheet that is coincident with the $z = 0$ plane and centred at the origin of the co-ordinate system. As the sheet is perfectly conducting the electric field outside the aperture will be exactly zero. Hence the boundary conditions may be expressed as

$$f(x, y) = \begin{cases} E_0 & \text{when } |x| \leq a \text{ and } |y| \leq b \\ 0 & \text{elsewhere} \end{cases} \quad (2)$$

These simulated fields were transformed using the field equivalence principle to construct the surface of a partial plane, initially parallel with the x–y plane passing through the $z = 1$ m point. This plane was rotated by $\pm 30^\circ$ in azimuth about the origin of the antenna co-ordinate system, as illustrated in Fig. 4, to construct the field distribution plotted in Fig. 5, c.f. [7].

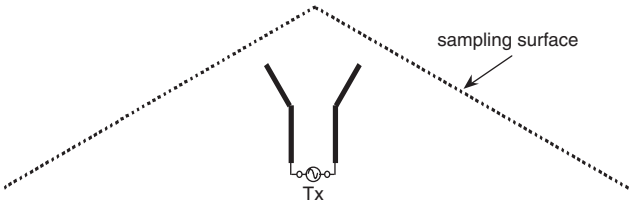

Fig. 4 *Schematic representation of aligned and misaligned antennas*

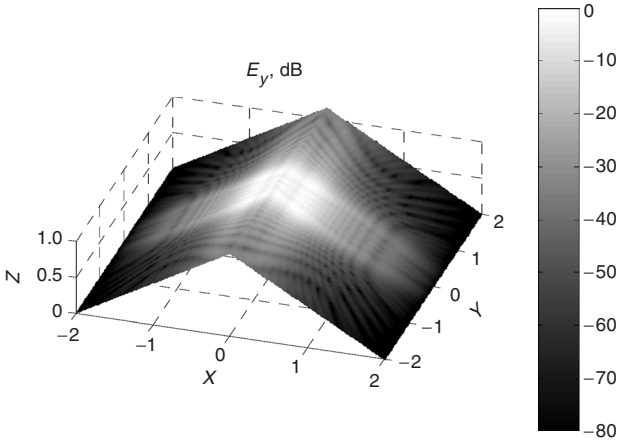

Fig. 5 *Grey-scale plot of simulated near-field power*

Figure 6 is a far-field plot comparing ideal far-field data and equivalent data derived from the two rotated partial plane near-field data illustrated. The agreement between the respective cuts is good with differences only becoming apparent beyond $\pm 80^\circ$ where this is particularly apparent in the phase plot. These differences have been found to result from the discontinuity encountered at the intersection of the two planes. Unfortunately with any symmetrical

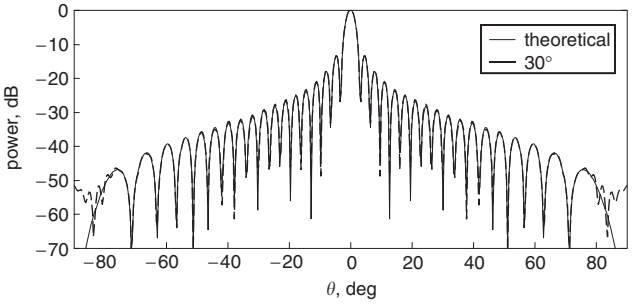

Fig. 6 *Comparison of far-field horizontal cuts of polyhedral transform and theoretical patterns*

biscan configuration the intersection between the adjacent partial scans lies in the region of greatest field intensity.

4.2 Triscan auxiliary rotation technique

The triscan configuration is a practical candidate for a polyplanar system as the intersection between adjacent partial scans can be chosen to be away from regions of high field intensities. To this end the near-field measurement geometry was simulated using the field equivalence principle to construct the surface of a partial plane, initially parallel with the x–y plane. This plane was rotated by $\pm 30^\circ$ in azimuth about the origin of the antenna co-ordinate system to construct the field distribution shown in Fig. 7. This constitutes a desirable arrangement where the intersections have been chosen to be across a region of space in which the field intensities are typically more than 30 dB smaller than the largest signal. Figure 8 contains a great circle cut of the equivalent far-field vector pattern function compared with the ideal (theoretical) pattern. Unfortunately these results can be seen to be in error for very large angles i.e. those angles greater that 87° and stems from the discontinuity in the first derivative of the near-field data across the intersection between the partial scans.

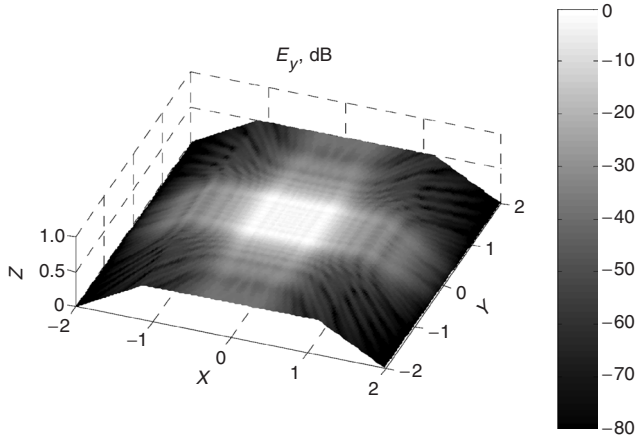

Fig. 7 *Grey-scale plot of simulated near-field power for triscan configuration*

An often-adopted technique for the quantitative comparison of antenna pattern data sets is the calculation of an equivalent multipath level (EMPL). This can be thought of as the amplitude necessary to force the different pattern values to be equal. Thus, it can be seen from Fig. 9 that the equivalent multipath level everywhere within the maximum look angle is low with the largest value being less than −60 dB and the value being typically less than −70 dB over

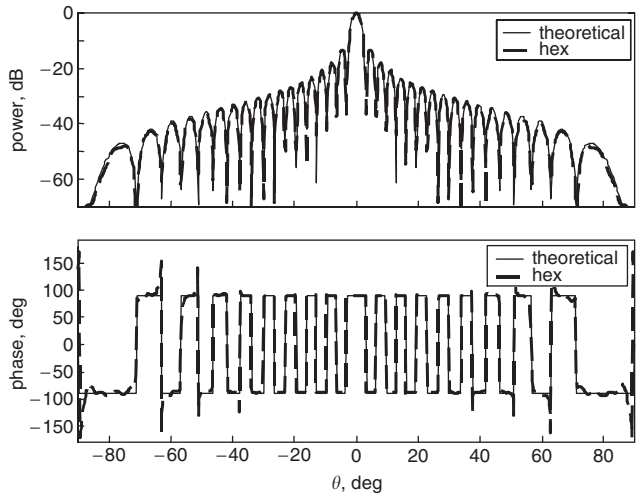

Fig. 8 *Comparison of far-field horizontal cuts of polyhedral transform and theoretical prediction*

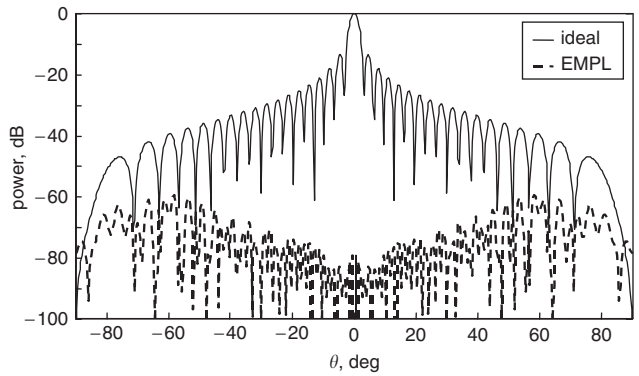

Fig. 9 *EMPL comparison showing agreement attained between results presented in Fig. 8*

the majority of the forward hemisphere which is approaching the practical noise floor of a typical planar facility.

The extent of the differences between the respective far-field patterns can be quantified with the evaluation of the coefficient of ordinal correspondence k. This is a single coefficient, independent of scaling or shift due to the differences in reference levels, derived from ordinal statistics, details of which can be found in [8]. Table 1 contains values of k that correspond to a conventional planar configuration, a biscan auxiliary rotation scheme (two planes inclined at $\pm 30^\circ$ and where the intersection is through the middle of the antennas peak field) and the modified triscan auxiliary rotation scheme. Here, if the two data sets are perfectly correlated, then $k = 1$, when the data sets are perfectly negatively correlated then $k = -1$ and when no relationship exists the magnitude of k tends to zero.

Table 1: Comparison *k*-values from various measurement configurations

Measurement	*k*
Conventional planar measurement	0.6372
Biscan auxiliary rotation scheme	0.5333
Triscan auxiliary rotation scheme	0.8088
Pentahedral-scan auxiliary	0.8154

The conventional planar measurement can be thought of as constituting the benchmark by which other novel schemes can be compared. The imperfect k value reflects the degradation of the far-field pattern that inevitably results from the introduction of spectral leakage caused by truncation of the near-field data set. Although the biscan configuration successfully increases the ability of a given facility to determine wide-out antenna performance, additional errors are introduced that result from the intersection of the partial scans. Clearly the triscan scheme can be seen to offer results that constitute an overall improvement to those supplied by conventional planar techniques.

The triscan scheme addresses the problem of obtaining wide-out azimuthal performance, but does not address the problem in the elevation plane. This can be readily resolved by rolling the AUT through $\pm 90^\circ$ about its mechanical boresight and repeating the measurement. This would not be suitable for all antennas and alternatively the AUT can be 'nodded' in elevation, then permitting data to be sampled over the surface of two additional planes. This procedure yields a polyplanar measurement consisting of five intersecting partial scans that when combined produce a sampling surface that resembles a flat-topped pyramid. Inspecting the degree of agreement for the pentahedral scan is now found to be encouraging with differences only becoming apparent at the -70 dB level or for a large polar angle. Table 1 further illustrates the degree of success of this technique with the pentahedral auxiliary rotation scheme offering the best performance. This technique is particularly applicable for instruments with a rectangular aperture plane as little power is delivered to intercardinal regions. For circularly symmetrical instruments, further validation is required.

4.3 Reconstruction of normal field component

Conventionally the normal field components are not measured, instead they are recovered from the tangential components via an application of the plane wave condition, i.e. $\underline{k} \cdot \underline{E} = 0$. If however, the sampled data set is truncated, the reconstructed normal field component will be in error. This is clearly a problem as partial scans are by definition truncated. Furthermore, this field component is required before the partial data sets can be combined, as the principal of superposition requires that each component be resolved onto the SAME polarisation basis. These difficulties can be resolved if the normal field component is sought over the surface of each partial plane. All three orthogonal field components can then be transformed to the far field whereupon the partial data sets can be combined in the usual way. Thus the normal field component over the partial scan plane can be expressed mathematically as

$$E_z(x, y) = -\Im^{-1}\left\{\frac{k_x \Im\{E_x(x, y)\} + k_y \Im\{E_y(x, y)\}}{k_z}\right\} \quad (3)$$

where $\Im$ represents the 2-D Fourier transform of the near field on a plane and $\Im^{-1}$ its inverse. Using the simulator the normal field component was obtained from the tangential components and results from this comparison can be found in Fig. 10*a*. The spurious high-frequency ripple present in the reconstructed normal field component can be removed by windowing the tangential field components before transforming to the angular spectrum. The 'convoluted' normal spectral component can be obtained directly from the plane-wave condition whereupon it can be inversely transformed to obtain the 'windowed' normal field component. The windowing function can then be divided

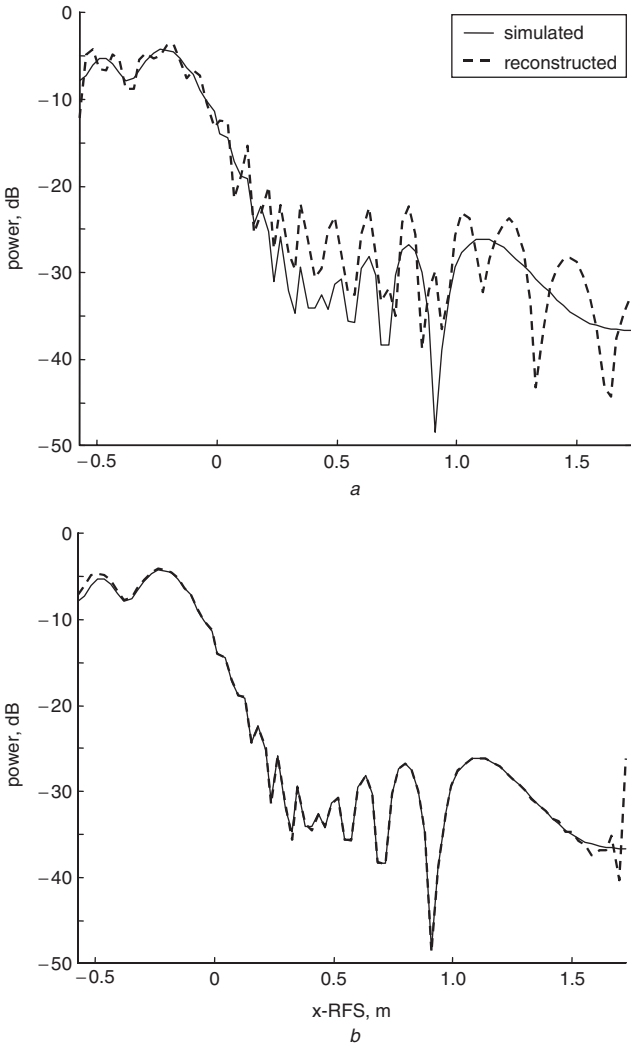

Fig. 10 *Plot of simulated and reconstructed normal field component*
a Without windowing
b With windowing

out to obtain reliable results such as those presented in Fig. 10*b*. The derivation of the expressions that are used to correct the measured near-field data for the directive properties of the measuring probe relied on the validity of the plane-wave condition. Thus the normal field component utilised implicitly within these expressions will be recovered erroneously for the case where the near-field data set is truncated. Thus truncated measurements that are corrected with these expressions will also be in error. Again, such difficulties can be avoided with the application of a suitable windowing function. A proof of the validity of the use of windowing functions to obtain reliable longitudinal field components can be found presented in the Appendix. Using a similar approach a proof demonstrating the validity of the use of windowing functions when applying probe pattern correction can be obtained.

Various windowing functions have been tried and the best results have been obtained by utilising a Bartlett [9] i.e. a triangular, windowing function. At the extremities, this technique gradually becomes susceptible to noise and at the perimeter suffers from a divide by zero error. This can be overcome by over-scanning the data where adjacent planes join. Figure 11 shows a far-field copolar azimuth cut for a representative triscan auxiliary rotation configuration for a 0, 5, and 20 column over-scan configuration. Clearly, the

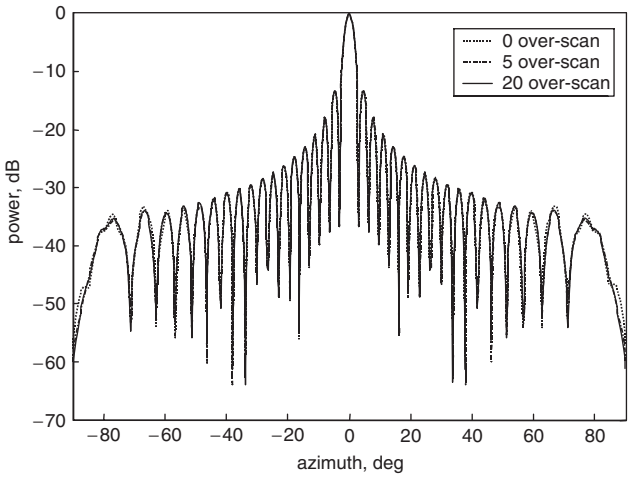

Fig. 11 *Comparison of far-field horizontal cuts of polyhedral transform for various degrees of over-scan*

over-scan configurations improve the quality of the results obtained. This is most observable at wide angles, however an over-scan of greater than five columns appears to offer only a very limited improvement.

Within the most general integral transform derivation of the plane-wave spectrum (PWS) representation of electromagnetic fields [10], the partial derivatives of the boundary conditions with respect to the x-axis are obtained using the following operator substitution:

$$\frac{\partial u(x,y,z)}{\partial x} = \Im^{-1}\{-jk_x\Im\{u(x,y,z)\}\} \tag{4}$$

A similar expression can be obtained for the y partial derivative, and higher-order derivatives were obtained by successive applications of these operator substitutions. These expressions were assumed to hold everywhere and were employed to reduce the scalar Helmholtz equation, which is a second-order partial differential equation, to an ordinary differential equation. Unfortunately, if the boundary conditions are only piecewise smooth the integration by parts performed within the derivation of these operator substitutions becomes impossible. The implication of this is that the function must be considered as a distribution, i.e. a generalised function, and crucially, any derivatives must also be considered as generalised derivatives. This can be easily demonstrated as the far electric field in a half-space at stationary points of the first kind can be obtained rigorously using spectral techniques from near-field data sampled over a nonplanar aperture using [11]

$$E(r\underline{\hat{u}}) = j\frac{e^{-jk_0r}}{\lambda r}\int_{-\infty}^{\infty}\int_{-\infty}^{\infty}E(x,y,z)e^{jk_0(\alpha x+\beta y+\gamma z)}(\underline{\hat{u}}\cdot\underline{\hat{n}}) \times\sqrt{\left(\frac{\partial g}{\partial x}\right)^2+\left(\frac{\partial g}{\partial y}\right)^2+1}\,dxdy \tag{5}$$

Here the surface profile is expressed as a function of the plaid, monotonic, and equally spaced co-ordinates x and y where $g(x,y,z) = z - f(x,y) = 0$, $\underline{\hat{n}}$ is the outward facing unit normal to the surface of integration and $\underline{\hat{u}} = \alpha\underline{\hat{e}_x} + \beta\underline{\hat{e}_y} + \gamma\underline{\hat{e}_z}$ is the unit vector in the direction of the stationary point. Here, provided the fields are sampled at, or preferably higher than, the Nyquist rate over the sampling surface, and provided the surface of integration is smooth, i.e. the function describing the surface profile, and all of the first partial derivatives are continuous, reliable far-field data can be obtained. However, as soon as the surface profile is

not smooth, as is the case for the polyplanar technique, a spurious high-frequency ripple can be observed. The amplitude of this ripple is dependent on the magnitude of the ordinary discontinuity and the intensity of the field in that region. Although useful for electromagnetic modelling, and illustrating the difficulties inherent within the PWS method, these expressions are not in a form that is applicable for near-field antenna measurements as no provision is made for probe pattern correction.

5 Polyplanar transformation algorithm

A certain degree of success has been obtained by acquiring near-field data over the surface of a flat-topped pyramid. Here the intersection between adjacent scans can be chosen to be regions of lower field intensities, and the angle between scans could be made to be small typically a few tens of degrees. However, in principle, these techniques only minimise but do not remove the error inherent within the transformation technique. Consequently an alternative technique that better handles discontinuities in the sampling surface was sought. To this end the Kirchhoff–Huygens (KH) formula was utilised [12]. This method essentially constitutes a direct integration of Maxwell's equations with the use of a vector Green's theorem. The choice of the field form of this method was thought to be preferable in this case as, although an equivalent surface electric and surface magnetic current form of the KH formula exists and is widely used, the quantities that are sampled within the measurement are proportional to fields, not surface currents. Despite the fact that the KH method has been utilised here, in theory any field propagation formula could be employed provided that it can be used with fields sampled over surfaces that are not smooth. Unfortunately, in addition to being computationally more intensive than the spectral method, the KH method requires that both the electric and magnetic fields be known over the sampling surface. Thus the filtered probe corrected PWS method can be utilised to correctly recover the normal component of the electric field and the magnetic field components can be reconstructed over each of the partial scans. When combined these partial scans form a conceptual finite but unbounded surface that encloses all of the current sources. This data can then be transformed to the far field using the KH method. Figure 12 shows a block diagram of the novel hybrid spectral physical optics transformation algorithm.

6 Experimental verification

The fully absorber lined facility used to verify the technique contains a planar positioner of an inverted-T design fabricated by Near-Field Systems Inc. (NSI). This design was chosen so that the scattering cross-section of the frame could be minimised. The relatively small physical dimensions of the scan plane, approximately $1\,m^2$, enable the planarity of the scanner to be maximised. Other advantages include minimising the length of the RF cabling within the facility. As highly phase-stable cable is often relatively lossy at $1\,dBm^{-1}$ the short length of the cable runs enables the dynamic range of the facility to be maximised, which is crucial when the AUT is not nominally aligned to the axes of the range. Since the scanner is small and light it is also very fast with a maximum scan speed of 0.5 m/s thus acquisition times are short, typically of the order of a few minutes, so very little thermal drift is present within a given acquisition. The RF subsystem is based around an HP8720 vector network analyser.

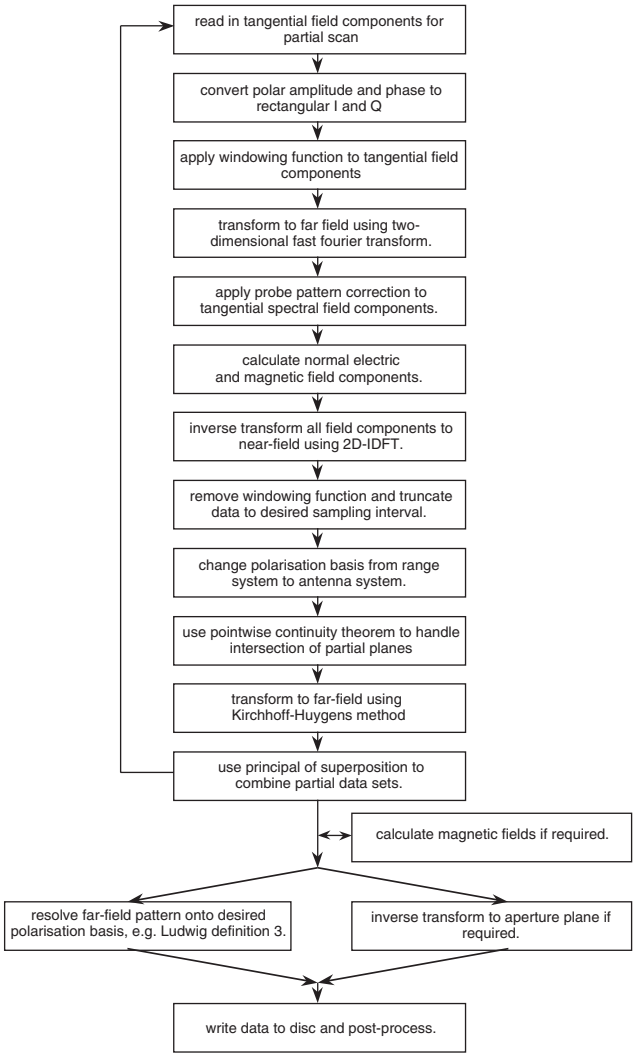

Fig. 12 *Block diagram of auxiliary rotation near-field to far-field transform algorithm*

In an attempt to verify the polyplanar measurement and transformation methodologies a cubic geometry was adopted, as the orthogonality between adjacent partial scans would constitute a worst-case scenario while being relative simple to realise. The AUT positioner was fabricated from a thin absorber-clad steel column on which the AUT could be mounted precisely in one of six discrete orientations. A relatively low-gain x-band corrugated horn was chosen as the AUT as this class of antenna is conventionally thought to be unsuitable for characterisation by planar techniques.

With the antenna operating at 10 GHz, the x- and y-polarised electric field components were sampled using a square acquisition window of $-0.425\,m \leq x_{RFS} y_{RFS} \leq 0.425\,m$ with a range length, i.e. an AUT-to-probe separation of 0.282 m. Since the intention was that the tangential components of the near electric field were to be sampled over the surface of a cube, this corresponded to an over scan of 12 elements, i.e. approximately six wavelengths, around the perimeter of the square acquisition window. Once the x- and y-polarised near-field components had been sampled the AUT was rotated by 90° in azimuth so the second side of the cube could be measured. All six surfaces of the cube were sampled by performing the following rotations: AUT nominally aligned to axes of range; positive rotation of 90° about y-axis; negative rotation of 90° about y-axis; positive rotation of 180° about

y-axis; positive rotation of 90° about z-axis followed by a positive rotation of 90° about new x-axis; and positive rotation of 90° about z-axis followed by a negative rotation of 90° about new x-axis. The requirement for the inclusion of the back plane follows from the requirement to perform the pattern integration over a closed surface. Although utilising the line charge distribution method [13], often referred to as the Kirchhoff–Kottler formulation, can ease these difficulties this technique has not yet been implemented. In practice, it is not possible as a degree of truncation will inevitably result from the positioning system; this example was chosen to verify the transformation process rather than the measurement process.

Each of the six partial scans were processed using the novel transformation algorithm described. The y-polarised electric nearfield can be found plotted in Fig. 13 and as expected the fields at the intersection between adjacent partial scans are continuous. Similarly encouraging results were obtained for other polarisations and for the magnetic fields. These data sets were subsequently transformed to the farfield and resolved onto a Ludwig III polarisation basis. Great-circle cardinal cuts are shown in Fig. 14. Here, the black traces represent patterns obtained from the polyplanar technique while the dashed traces denote results obtained from the Queen Mary compact antenna test range (CATR) [14]. The high-frequency oscillatory behaviour evident within the azimuth cut of the CATR at wide angles is a result of a multiple reflections within the facility and should be ignored.

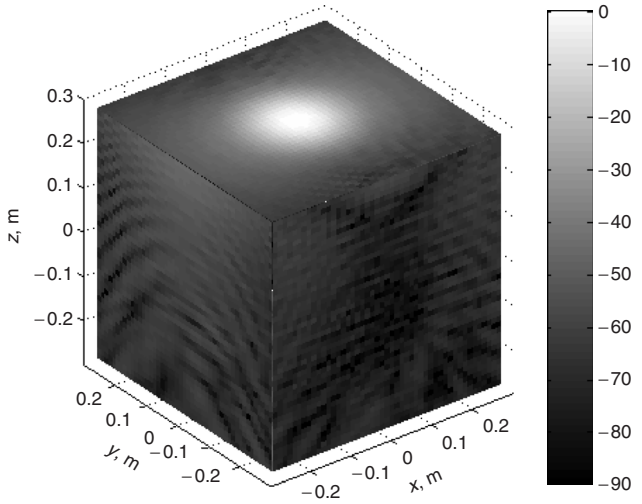

Fig. 13 *Probe corrected y-polarised electric field component*
Frequency = 10 GHz

As described previously, the six partial planes will not intersect perfectly, and the adverse effects of reflections from scatters within the NF chamber will degrade the resulting far-field patterns. Corrugated horns are renowned for their symmetry. Consequently lack of symmetry can often be used as an indication that a measurement is unreliable. Here, although a good degree of symmetry can be observed in the azimuth plane, the elevation cut clearly contains a number of asymmetries. This difference between the cardinal cuts is most probably an artefact of additional rotation required to sample the top and bottom planes of the cube, as the additional 90° rotation will inevitable introduce further alignment errors. As the AUT is located at the centre of a conceptual measurement cube, classically the angle of validity for the front plane would be $\pm 45°$ in

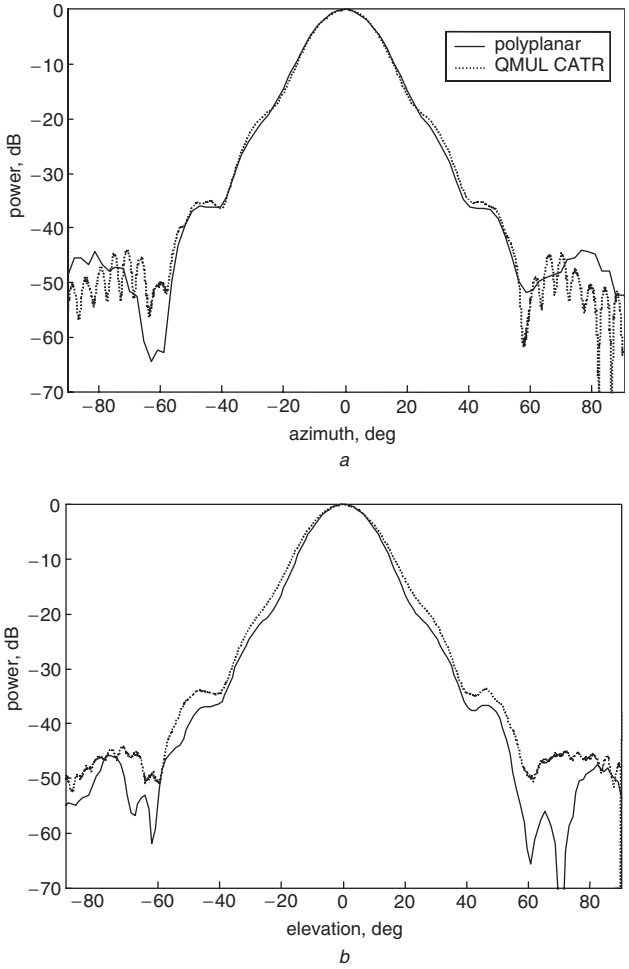

Fig. 14 *Great circle cardinal cuts*
a Azimuth
b Elevation

azimuth and elevation. Thus particular attention should be paid to regions around $\pm 45°$ as if the transformation were in error, this is where it would be expected to be most noticeable. Crucially no discernible divergence is observable in this region. Finally, the radial component of the far electric and magnetic fields were calculated. As expected these components were found to be reassuringly small with a peak signal of approximately 150 dB below the copolar peak.

7 Conclusions

The measurement process still requires a great deal of refinement. However, for the first time, encouraging results that are free from the high-frequency spurious ripples that have plagued all previous attempts have been obtained. Thus it would appear that probe corrected spectral techniques could be combined with the KH method to form a hybrid technique that alleviates the deficiencies that render these techniques useless when used individually. This paper has shown through numerical simulation and experimental measurement that a flat-topped pyramid provides a possible solution to the measurement of high-gain antenna patterns in the forward hemisphere using a planar scanner of size of order 1.5 times the size of the radiating aperture. Additionally it has been shown that by enclosing a medium-gain antenna (e.g. a corrugated horn) within an imaginary box and measuring the near field on all

six sides of the box, using a suitable rotation of the AUT, a prediction of the full spherical radiation pattern of the antenna can be obtained.

8 Acknowledgments

The authors wish to acknowledge the financial support from the UK EPSRC in respect to the provision of the near-field measurement facility at Queen Mary, University of London. The writers gratefully acknowledge the helpful suggestions made by the reviewers.

9 References

1 Kerns, D.M.: 'Plane-wave scattering-matrix theory of antenna and antenna–antenna interaction'. National Bureau of Standards (US) Monograph 162, 1981
2 Silver, S.: 'Microwave antenna theory and design' (McGraw-Hill, New York, 1949), Section 3.8
3 Balanis, C.A.: 'Antenna theory analysis and design' (Wiley, 1997), Chap. 16, p. 852
4 Newell, A.C.: 'Planar near-field antenna measurements'. National Bureau of Standards (US) Technical Note, p. 93
5 Hsu, H.P.: 'Applied Fourier analysis' (Harcourt Brace, 1967), p. 45
6 Gregson, S.F., and Robinson, A.J.: 'An interrange comparison in support of the characterisation of space antenna systems and payload testing'. Presented at the IEE Colloquium on Antenna Measurements, 17th June 1988
7 Gregson, S.F., McCormick, J., and Parini, C.G.: 'Measuring wide angle antenna performance using small planar scanners'. Presented at the Int. Conf. on Antennas and Propagation, ICAP, 2001
8 Gregson, S.F., McCormick, J., and Parini, C.G.: 'Advances in the objective measure of comparison between antenna pattern functions'. Presented at the Int. Conf. on Antennas and Propagation, ICAP, 2003
9 Harris, F.J.: 'On the use of windows for harmonic analysis with the discrete Fourier transform', *Proc. IEEE*, 1978, **66**, pp. 66–67
10 Gregson, S.F.: 'Probe-corrected polyplanar near-field antenna measurements'. PhD thesis, University of London, 2003, p. 21
11 Gregson, S.F., Parini, C.G., and McCormick, J.: 'Wide angle antenna pattern measurements using a polyplanar near-field technique'. Presented at the Int. Conf. on Antennas and Propagation, ICAP, 2003
12 Clarke, R.H., and Brown, J.: 'Diffraction theory and antennas' (Ellis Horwood, 1980), p. 227
13 Collin, R.E., and Zucker, J.: 'Antenna theory' (McGraw-Hill, 1969)
14 Olver, A.D., and Parini, C.G.: 'Milimetrewave compact antenna test ranges'. Presented at JINA, Nice, November 1992

10 Appendix: Plane-wave condition

The normal field component is obtained from the tangential field components by applying the plane-wave condition to the far-field electric field or to the angular spectra

$$E_n = -\frac{\underline{k_t} \cdot \underline{E_t}}{k_n} \tag{6}$$

where E_n is the electric field component at a normal to the measurement plane, and k_n is the component of the propagation vector that is normal to the measurement plane. Similarly, E_t is the component of the electric field vector that is tangential to the measurement plane. This will be successful if the near-field data set is free from truncation. If however the sampled data set is truncated, and by definition partial scans are truncated, then the reconstructed normal field component will be in error. These difficulties can be resolved if the normal field component is sought only over the surface of each partial plane as windowing functions can be utilised while maintaining the integrity of the underlying function.

The normal field component over the partial scan plane can be expressed mathematically as

$$E_z(x, y) = -\mathfrak{I}^{-1}\left\{\frac{k_x\mathfrak{I}\{E_x(x, y)\} + k_y\mathfrak{I}\{E_y(x, y)\}}{k_z}\right\} \tag{7}$$

Here $\mathfrak{I}$ is taken to denote the Fourier operator and $\mathfrak{I}^{-1}$ its inverse. For example, with the time dependency suppressed, a two-dimensional Fourier transform of the field function can be defined by the integral

$$\begin{aligned}\underline{F}(k_x, k_y) &= \mathfrak{I}\{\underline{E}(x, y)\} \\ &= \int_{-\infty}^{\infty}\int_{-\infty}^{\infty}\underline{E}(x, y)e^{j(k_x x + k_y y)}dxdy\end{aligned} \tag{8}$$

Similarly, the inverse can be expressed as

$$\begin{aligned}\underline{E}(x, y) &= \mathfrak{I}^{-1}\{\underline{F}(k_x, k_y)\} \\ &= \frac{1}{4\pi^2}\int_{-\infty}^{\infty}\int_{-\infty}^{\infty}\underline{F}(k_x, k_y)e^{-j(k_x x + k_y y)}dk_x dk_y\end{aligned} \tag{9}$$

Here $\underline{E}$ and $\underline{F}$ are vector analytic functions and the limits of integration collapse to the region of the partial scan plane for the spatial field function and to the region of visible space, i.e. where $k_0^2 > k_x^2 + k_y^2$, for the spectral field function. The near-field data set is first windowed before it is transformed to the angular spectrum. The normal field component is obtained by applying the plane-wave condition before the inverse transform is taken whereon the windowing function can be removed from the normal component. This can be proved as follows.

The derivation aims to establish analytically that the normal field component can be obtained from the tangential field components when the angular spectrum is disturbed by the presence of an arbitrary, but known, windowing function. The plane-wave condition can be expressed in terms of the angular spectra as

$$F_z(k_x, k_y) = -\frac{\alpha}{\gamma}F_x(k_x, k_y) - \frac{\beta}{\gamma}F_y(k_x, k_y) \tag{10}$$

Here α, β and γ are the direction cosines in the x-, y- and z-axes, respectively, so that $\underline{\hat{u}} = \alpha\underline{\hat{e}_x} + \beta\underline{\hat{e}_y} + \gamma\underline{\hat{e}_z}$ where $\underline{\hat{u}}$ is a unit vector which is simply related to the direction of propagation $\underline{k} = k_x\underline{\hat{e}_x} + k_y\underline{\hat{e}_y} + k_z\underline{\hat{e}_z} = k_0(\alpha\underline{\hat{e}_x} + \beta\underline{\hat{e}_y} + \gamma\underline{\hat{e}_z})$. Consider the effect of applying a windowing function to each electric field component in the near field on the plane-wave condition in the angular spectrum

$$E_{xr}(x, y) = w(x, y)E_x(x, y) \tag{11}$$

$$E_{yr}(x, y) = w(x, y)E_y(x, y) \tag{12}$$

$$E_{zr}(x, y) = w(x, y)E_z(x, y) \tag{13}$$

Here the subscript r is used to denote a spatially windowed quantity. Thus by using the convolution theorem [4] the plane-wave condition when expressed in terms of windowed electric near-field components becomes

$$\begin{aligned}W(k_x, k_y) \otimes F_z(k_x, k_y) = &-\frac{\alpha}{\gamma}\left[W(k_x, k_y) \otimes F_x(k_x, k_y)\right] \\ &-\frac{\beta}{\gamma}\left[W(k_x, k_y) \otimes F_y(k_x, k_y)\right]\end{aligned} \tag{14}$$

Here the spatial and spectral windowing functions, w and W respectively, are related through the Fourier operator. Hence

$$F_{zr}(k_x, k_y) = -\frac{\alpha}{\gamma}F_{xr}(k_x, k_y) - \frac{\beta}{\gamma}F_{yr}(k_x, k_y) \tag{15}$$

where

$$\begin{aligned} F_{xr}(k_x, k_y) &= \mathfrak{I}\{E_{xr}(x, y)\} \\ &= \mathfrak{I}\{w(x, y)E_x(x, y)\} \\ &= W(k_x, k_y) \otimes F_x(k_x, k_y) \end{aligned} \tag{16}$$

Similar expressions can be formed for F_{yr} and F_{zr}. Thus

$$\begin{aligned} F_{zr}(k_x, k_y) = &-\frac{\alpha}{\gamma}\mathfrak{I}\{w(x, y)E_x(x, y)\} \\ &-\frac{\beta}{\gamma}\mathfrak{I}\{w(x, y)E_y(x, y)\} \end{aligned} \tag{17}$$

Hence the reconstructed normal component can be expressed reconstructed from

$$\begin{aligned} E_z(x, y) = &\frac{1}{w(x, y)}\mathfrak{I}^{-1} \\ &\times \left\{-\frac{\alpha}{\gamma}\mathfrak{I}\{w(x, y)E_x(x, y)\}\right. \\ &\left.-\frac{\beta}{\gamma}\mathfrak{I}\{w(x, y)E_y(x, y)\}\right\} \end{aligned} \tag{18}$$

This holds for any windowing function that is both absolutely integrable and non-zero.